A comprehensive study of structural and optical properties of ZnO bulk crystals and polycrystalline films grown by sol-gel method

Ewelina Nowak[1] · Miroslaw Szybowicz[1] · Alicja Stachowiak[1] · Wojciech Koczorowski[1,2] · Detlev Schulz[3] · Kazimierz Paprocki[4] · Kazimierz Fabisiak[4] · Szymon Los[4]

Abstract

The presented article concerns the comparison between two different zinc-oxide structures - bulk crystals and polycrystalline thin films. Bulk crystals were grown by a Bridgman method. For thin-film production, a sol-gel spin-coated method was chosen. A part of thin layers samples was annealed in 600 ^oC to induce recrystallization. The morphological and structural properties of all samples were investigated using various microscopy techniques, X-ray diffraction, and Raman spectroscopy. Confocal and scanning electron microscopy, as well as XRD, was used to estimate the influence of the recrystallization process on the morphology of the samples. The Raman vibrations in different scattering geometries were determined using polarized Raman spectra. What is more, in the case of the non-annealed sol-gel layer, the localized reorientation of crystallites was observed, using Raman microscopy. The morphology of the samples was compared to their optical properties, which were investigated by exploiting UV-Vis absorption and photoluminescence spectroscopy. Absorption spectroscopy allowed us to estimate the energy bandgap for different types of ZnO layers and to compare the values obtained for the ZnO crystal structure obtained by the Bridgman method. The photoluminescence and Raman spectroscopy were used to determine the possible defects correlated with the growth conditions.

Keywords ZnO · Sol-gel · Raman microscope · Structural study · Spectroscopy

1 Introduction

For the past few decades, dramatic advances in the research focused on finding and preparing the best materials for optoelectronics have been noticed. Due to their wide, direct bandgap, II-VI compounds seem to be perfect candidates for the application in innovative electronics. Even nowadays these materials are used in light-emitting devices in the short-wavelength region of the visible range [1].

✉ Miroslaw Szybowicz
miroslaw.szybowicz@put.poznan.pl

[1] Faculty of Materials Engineering and Technical Physics, Poznan University of Technology, Piotrowo 3, 60-965 Poznan, Poland

[2] Center for Advanced Technology, Adam Mickiewicz University, Umultowska 89C, 61-614 Poznan, Poland

[3] Leibniz-Institut fur Kristallzchtung, Max-Born-Strasse 2, 12489 Berlin, Germany

[4] Institute of Physics, Kazimierz Wielki University, Weyssenhoffa Sq. 11, 85-072 Bydgoszcz, Poland

Additionally, because of high-voltage blocking capability, high-temperature operation and high switching frequencies, most of the wide bandgap semiconductors may be feasibly used in power electronics [2].

One of the most promising II–VI semiconductors is zinc oxide (ZnO). ZnO in its most thermodynamically stable form, wurtzite-type structure, exhibits a wide bandgap at around 3.3 eV [3, 4]. In comparison with gallium nitride, another semiconductor with similar forbidden energy, this material possesses a strong polar binding, a large exciton binding energy (60 meV), and relatively high LO phonon energy of 72 meV [5]. Due to the oxygen and zinc atoms interlaced along the c-axis, wurtzite-type ZnO is polar in this direction – thus, the semiconductor has piezoelectric properties. As grown, ZnO evinces the n-type conductivity [6], nevertheless, the methods of n- and p-doped thin film deposition are being developed for decades.

Due to the described properties, the ZnO and its alloys are considered to be a great candidate for light-emitting and laser diodes, which cover the range from the green over the blue to the near-UV [4]. Undoped ZnO layers exhibit the

high electron concentration and insensitivity to visible light, therefore, they appear to be suitable as a semiconductor in thin-film transistors [4] or a transparent conductive oxide for photovoltaics [7]. Furthermore, in comparison with ITO films, ZnO layers are chemically stable, can be safely fabricated at low-cost, and are harmless to living organisms [8]. Piezoelectric and ferroelectric properties of ZnO films allow them to apply in acoustoelectronic, acoustooptic, and memory devices [9]. ZnO structures doped with transitional 3d-metals exhibit high Curie temperature, therefore, they are suitable for spintronics [8].

In optoelectronics, ZnO is commonly used as a thin film or single crystals. As the optical character of the material depends on its thickness and the preparation process [10], the main goal of this work is to compare the structural and spectral properties of ZnO layers applied on a glass substrate with a bulk crystal.

It is well-known that various techniques of ZnO film growth were developed. Thus, layers were successfully produced with methods such as RF-magnetron sputtering, pulsed laser deposition, and metal-organic chemical vapor deposition [8]. In case of the presented experiment, the aim was to prepare the material at the lowest cost. Due to the easily controlled chemical composition, the possibility of using reagents with low invasiveness to the environment, relatively low crystallization temperature [10], and the application without vacuum [8], the sol-gel spin-coating technique was chosen for the film's preparation. The bulk crystals were grown in the Leibniz Institute of Crystal Growth using the Bridgman method with inductively heated crucible with (0001) growth plane [11].

2 Material and methods

2.1 The growth of monocrystal

Bulk crystals were grown from the melt by the Bridgman method, which has already been detailed in the literature [12, 13]. The setup consisted of an RF-coil heated iridium crucible surrounded by insulating media. During the process, the chamber was filled with a high-pressure oxygen atmosphere to decrease the evaporation rate of zinc oxide - due to the oxygen evaporation the remaining zinc can easily react with iridium. It is worth noticing that the overpressure was supplied by carbon dioxide that decomposed at high temperatures. Before starting the process of premelting, the ZnO powder was compressed by cold isostatic pressing at a pressure up to 2000 bar and heated at 1100 ^{o}C for one day. At the beginning of the growth process, the compressed material was step heated up to a temperature above its melting point (T≈1975 ^{o}C). The next step involved adjusting the axial temperature gradient by changing the position of the crucible. This was accompanied by a constant temperature at the control point which led to a melting of the seed. After the second homogenization, crystallization was initiated by closed-loop control of the temperature [12, 13]. Crystals of 33 mm in diameter were grown and (0001) wafers were polished mechanically on the O-face and Zn-face. After cutting, the wafers were annealed in the air at 1100 ^{o}C to improve the crystal quality [14].

2.2 Preparation of thin films

The vast number of methods of producing thin films of ZnO with the sol-gel technique were already described in the literature [15–21]. Within this research, the standard sol-gel method was modified in a way, that would provide samples at the lowest environmental cost. Therefore, reagents chosen for a solution had to have a possibly most neutral impact on living organisms or to be easily degradable.

The initial step of the preparation of the precursor solution was to dissolve 1.38 g of zinc acetate in 25 ml of ethanol. The mixture was left in an ultrasonic bath for about 30 minutes. After the zinc acetate crystals dissolved into a uniform white suspension, 2.7 molar solution of ethanolamine in ethanol was added. The prepared precursor was also left in the ultrasonic bath for about an hour to clear the solution, and annealed in 70 ^{o}C for 30 minutes.

As a substrate material, glass plates were used. The cleaning process of the substrates consisted of four steps: immersing in a solution of detergent and water, then Milli-Q pure water, followed by methanol and acetone in the ultrasonic bath, and eventually dried in hot air. After placing the substrate on the disc of the spin coater, the coating solution (approx. 0.5 ml) was dropped on the substrate at a spinning rate of 100 rpm and spin-coated in two steps with 1300 rpm for 25 s and 2300 rpm for 10 s. The obtained film was dried in the air at 110 ^{o}C for 5 min. This cycle was repeated 4 times for sample 4L_NA, 4L_A, and 9 times for sample 9L_A to obtain films with various thicknesses. Since annealing in higher temperatures induces reorientation of crystallites [22, 23], samples 4L_A and 9L_A were annealed in a tube furnace for 1 hour in 600 ^{o}C to decompose the precursor and oxidize films [24]. Plates were left in a furnace until it was cooled down, which helped them to crystallize without superficial fissures and point defects [25].

Thorough denotations of the samples and details of their fabrication may be found in Table 1.

2.3 Instrumental analysis

The first part of the research was an analysis of the morphology of the samples. Surface topography and fluorescence were observed with a Zeiss LSM 710 confocal microscope with an argon laser at 488 nm as an excitation light source.

Table 1 Denotations and detailed specification of the samples. Rows: "Solution preparation", "Substrate preparation" and "Spinning conditions" refer to all samples

Sample	Solution preparation	Substrate preparation	Spinning conditions	Repetition	Annealing
4L_A	25 ml of zinc acetate solution in ethanol + 5 ml MEA (stirred for 1 h in the ultrasonic bath, aged for 0,5 h in 70 °C)	Glass substrate (Stages of washing: - Detergent solution - Milli-Q water - Methanol - Acetone - Hot-air drying	Dropping on a substrate at spinning rate of 100 rpm and spin-coated with 1300 rpm and 2300 rpm. Dried in the air in 110 °C for 5 min after deposition of each layer	4 times	1 h in 600 °C
4L_NA				4 times	not annealed
9L_A				9 times	1 h in 600 °C

Complementary measurements were conducted with a Scanning Electron Microscope. Both methods were used also for thin layers thickness estimation; the size of the bulk crystals was measured with the micrometer. The X-ray diffraction (XRD) patterns were recorded for the evaluation of the structural changes under the annealing influence. XRD was registered using DRON-4a, $\Theta - 2\Theta$ XRD diffractometer, where a Cu Kα X-ray tube was operated at a voltage of 36 kV and 18 mA current.

Due to its high sensitivity to the crystal structure, Raman microscopy measurements were conducted to provide more detailed information from the surface. Raman scattering was observed at room temperature using a Renishaw inVia system. The spectrometer was equipped with a Leica confocal microscope - for all measurements, a long-distance objective with 50 times magnification and an argon laser at 488 nm as excitation light source were applied.

For absorption measurements, Varian Cary 4000 with a halogen lamp was used. Photoluminescence spectra were obtained using a Hitachi F-4500 system equipped with the xenon lamp as an excitation light source. Both measurements were conducted at room temperature.

3 Results

To study different properties of the ZnO layers, samples were subjected to various characterization techniques. To determine surface topography, high-resolution micrographs of all samples were taken (Fig. 1). Each thin-film sample (Fig. 1a, b, c) exhibits discernible grains on the surface. It is noticeable, that the grains on annealed layers are more prominent and bigger, which may be correlated with the recrystallization process [23, 26]. All of the thin-film samples have visible, small pits on their surface-although, the heat-treated samples (Fig. 1a and c) have a more homogeneous structure in these areas than non-annealed one (Fig. 1b). The structure of bulk crystal (Fig. 1d) has some visible pits and holes. It may be possibly caused by the selected method for growing (pits usually appear during the growth from the melt) and processing - the sample was only mechanically polished.

For each sample, the statistical distribution of grain size was prepared from lengths of 1000 statistically chosen crystallites. All of the samples present a huge dispersion in crystallite length values. The non-annealed sample (Fig. 2b) exhibits much smaller crystallites than annealed ones (Fig. 2a and c). The thickest, 9 layered sample (Fig. 2c) has scarcely bigger crystallites than a 4-layered, annealed sample (Fig. 2a).

The crystal structures shared by ZnO are wurtzite, zinc blende, and rocksalt, although, under ambient conditions, the thermodynamically stable phase is that of the wurtzite one [27]. It is worth noticing that the zinc blende ZnO structure

Fig. 1 Micrographs made with confocal microscopy in material mode - for 4*L_A* (a), 4*L_NA* (b), 9*L_A* (c) and bulk crystal (d). All pictures were taken with 10x magnitude objectives
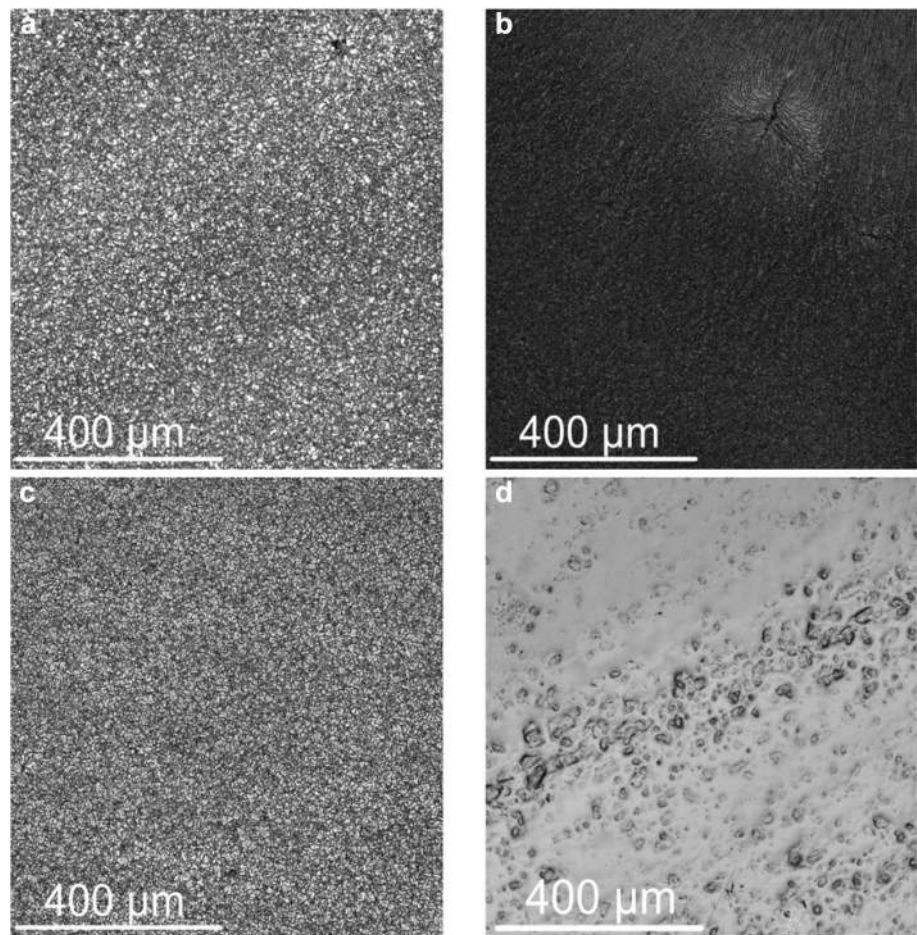

can be stabilized by epitaxial growth on cubic substrates, and the rocksalt may be obtained at relatively high pressures [27, 28]. To estimate samples symmetry and orientation, the X-ray diffraction and Raman spectroscopy were exploited. The XRD pattern of the ZnO layers is shown in Figure 3. For all measured samples, peaks (100), (002), (101), (102), (110), and (103) were detected. All detectable peaks can be indexed to the ZnO wurtzite structure and indicate the presence of crystallites with different orientations. This allows to conclude that the samples are polycrystalline. It is important to highlight the difference between patterns for annealed (Fig. 3 a, b) and non-annealed samples (Fig. 3 c), where the peak correlated with c-axis orientation (002) has a substantially lower intensity. This feature may indicate the re-orientation of crystallites under the recrystallization [29]. Since the crystal samples were investigated elsewhere [11], the measurement was not repeated. Due to the following article, samples exhibit {1120} orientation.

Raman spectroscopy was used as the leading method for the estimation of the crystal and the crystallites symmetry. The peaks characteristic for the hexagonal structure were observed in bulk crystals, as well as in thin films. The wurtzite structure ZnO unit cell consists of four atoms, therefore,

the crystal exhibits 12 phonon branches: 3 acoustic modes (LA and 2 TA) and 9 optical modes (3 LO and 6 TO). There are 6 optical phonon normal modes at Γ point: A1 + E1 + 2B1 + 2E2 [28], where the B1 are silent modes, the A1 and E1 are both Raman and infrared active, whereas the E2 modes are Raman active only [22, 23]. Furthermore, the A1 and the E1 modes are polar; their vibrations polarize the unit cell, which results in the generation of a long-range electrostatic field. As a result, the polar modes split into longitudinal optical and transverse optical components [30]. The Raman mode observed in a spectrum depends on the Raman selection rules, which consider the crystal orientation in relation to the direction and polarization of the incident and scattered light. This dependence is shown in Fig. 4, which present the spectra for different orientation of the ZnO monocrystal and different polarization of the light. In the case of measurements conducted for the growth-plane, the nonpolar E2 (high) mode was the main mode in the spectra (437 cm^{-1}). For the E2 (high) mode the Zn sublattice in the unit cell is essentially stationary, while the atoms of the O sublattice are vibrating in relation to each other [31]. The E2 (high) mode was detected in spectra registered from a cross-section of ZnO monocrystal with the incident and scattered
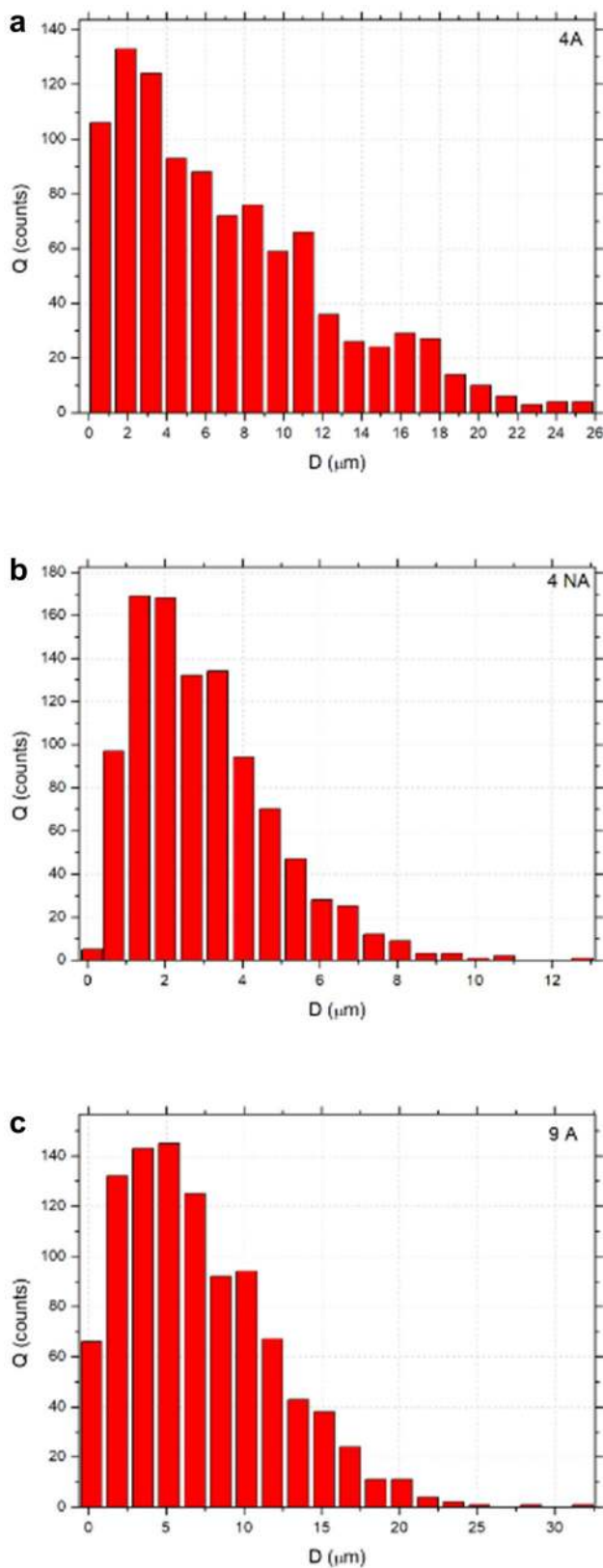
**Fig. 2** Distribution of grain size for 4*L_A* (a), 4*L_NA* (b) and 9*L_A* (c)
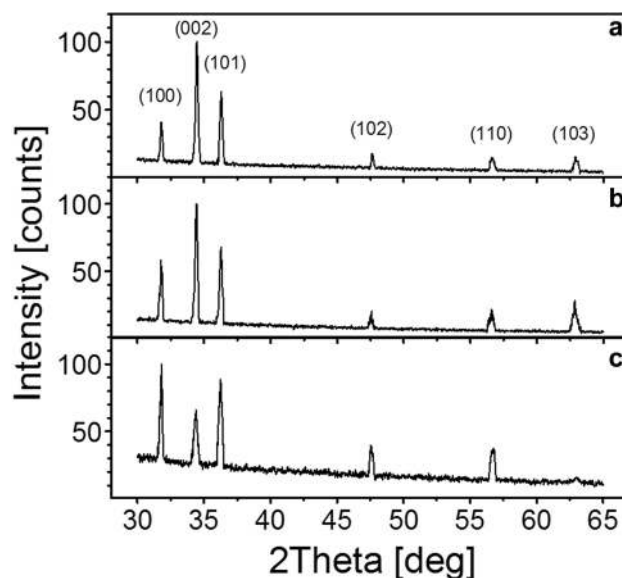
Fig. 3 XRD pattern of sample 9L_A (a), 4L_A (b), 4L_NA (c)

light polarized vertically to the c-axis. Spectra, where the E2 (high) mode was not present, show the E2 (low) mode (which represents the vibration of the Zn sub-network) at 200 cm^{-1}.

The A1 and E1 modes originate from oscillations of the two rigid sublattices. The A1 mode is parallel to the c-axis; the vibration of E1 mode spreads perpendicularly to the c-axis [31]. The twofold degeneracy of the E1 phonons is lifted except for phonon propagation along the c axis. For phonon propagation in the plane perpendicular to the c-axis, there will be an A1 transverse, an E1 transverse, and E1 longitudinal compounds [32]. The A1(TO) mode exhibits in the most spectra for cross-section, although it is extinguished at the spectrum for vertical polarization of incident light to c-axis and horizontal polarization of scattered light to the c-axis. The E1(TO) mode appears mostly for perpendicular polarization of the incident and scattered light and vanishes when the polarizations are parallel. This mode is forbidden in a backscattering geometry from both the a- and the c-faces of the wurtzite structure [30]. Although, a low signal from E1(LO) mode comes into sight for the horizontal polarization of incident light. A weak A1(LO) mode in c-plane spectra appears only for the polarization of incident light parallel to the polarization of scattered light.

The second harmonic of TO modes is present only for cross-section spectra with incident light polarized horizontally to the c-axis. 2LO and 2A1(LO)-2E1(LO) modes appear for most spectra (except for the spectrum recorded for the perpendicular polarization of the incident and scattered light).

Raman spectra of sol-gel ZnO thin layers are depicted in Figs. 5 and 6. Because of the possible thermal degradation of
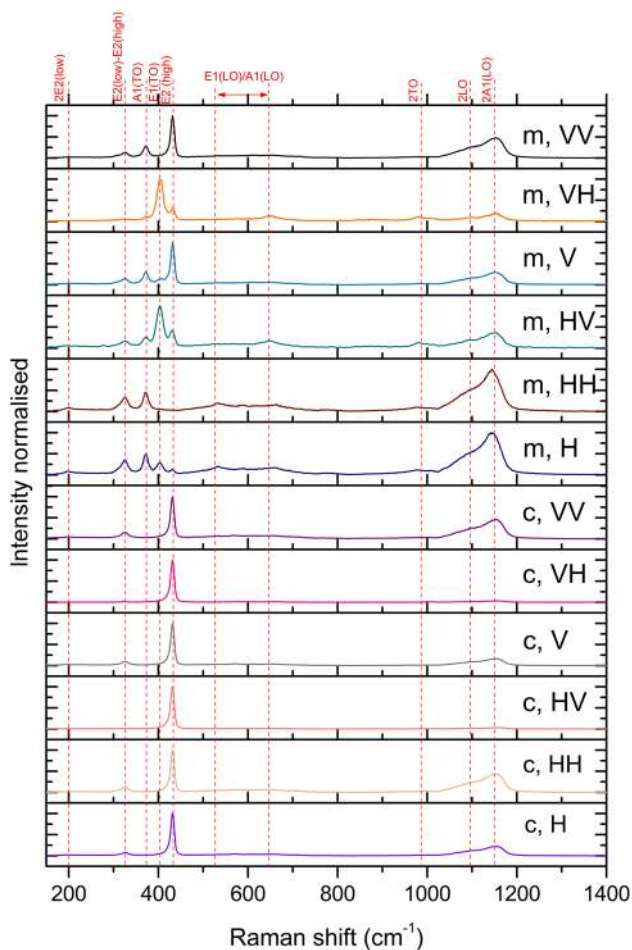
Fig. 4 Polarized Raman spectra for a bulk crystal of ZnO. c, m - crystal axis perpendicular to E; H - horizontal polarization, V- vertical polarization, 1st letter - polarization of incident light, 2nd - polarization of scattered light
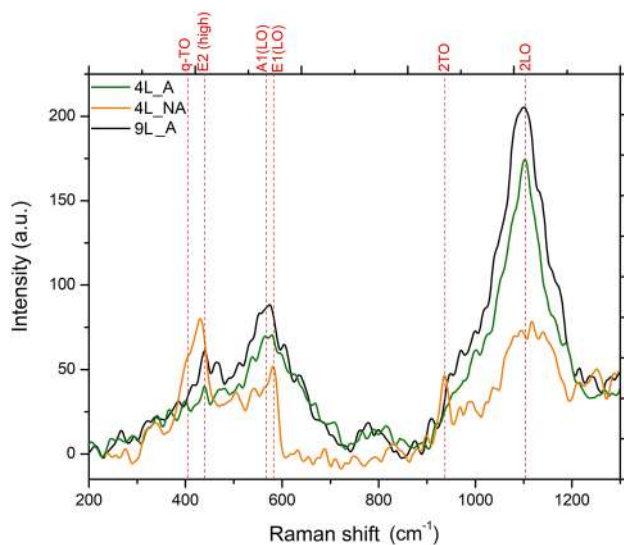
Fig. 5 Raman spectra of sol-gel thin films
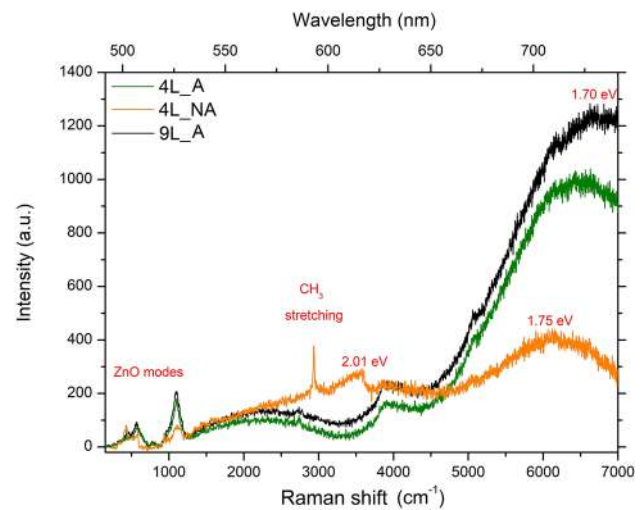
Fig. 6 Raman spectra of sol-gel thin films in a wider range

the material, all samples were measured using a 10mW laser beam. Thin films show slightly different spectra, which can be correlated with uncontrolled propagation of light. Analyzing single spectra for annealed samples one can observe peaks at 437, 570, 790, and 1100 cm^{-1} [32, 33], which could be assigned to modes E2, A1(LO), A1(LA+LO) and A1(2LO). In general, the A1(LO) is an allowed mode from the c-face in a backscattering geometry - the presence of this mode strongly points the crystallization with the c-plane as a growth-plane [30, 32].

A slightly different picture appeared for the non-annealed sample. For this specimen, the surface was very non-homogeneous. What is more, for most of the analyzed regions the TO quasimode situated near 400 cm^{-1}, it's second-order (990 cm^{-1}) and LO quasimode, which lies at 588 cm^{-1} were observed. The quasimodes are mixed symmetry modes in uniaxial crystals due to phonons propagating between the a- and the c- axes [32, 34]. Due to proximity to the position of E1(LO) mode, it was estimated that these regions had {1100} growth surface [34, 35].

Figure 6 shows the Raman spectra of the thin films in a wider range. The main differences between samples appear in the fluorescence range. As it may be noticed, the luminescence background is much more intensive in annealed samples. According to the literature, the red fluorescence can be correlated with the fact, that due to the heating treatment under oxygen-rich conditions, these samples were strongly oxidized [36, 37]. The red emission is usually explained by the electron transition from the conduction band to defect levels, or from the surface states to the valence state of the inner layer of the crystalline grain [38]. Its enhancement in annealed samples may be correlated with the generation of the defects between crystalline grains in the agglomerating procedure. Likewise, the influence of carbon contamination

on a luminescence background cannot be excluded. Carbon is always present as an unintentional dopant introduced during the growth of ZnO [39]. Furthermore, the method of growth was based on organic compounds, which could be a source of carbon defects in structures of thin films. Due to annealing in the oxygen-rich ambient, the carbon on the zinc side (C_{Zn}) defects may be predicted. On the other hand, in oxygen-rich annealing ambient, the carbon in ZnO thin film might react with oxygen to form CO/CO_2, which in turn reduces carbon concentration [39].

The spectrum of the non-annealed sample exhibits a suppressed red luminescence. For a larger part of the non-annealed sample surface, a peak at 2934 cm^{-1} was recorded. This band can be assigned to CH_3 stretching, which provides the information, that organic substances from a precursor solution did not evaporate fully. As can be seen in Fig. 7c, where the ratio of the intensity of 2934 cm^{-1} to 1110 cm^{-1} peak can be seen, the surface of the sample has significant differences in ratio values, thus it can lead to an estimation, that the residual organic substances are distributed heterogeneously.

In Fig. 7a and 7b, one can observe the ratio of the intensity of characteristic peaks for different orientations of crystals. For the analyzed surface, the most prominent peak was TO quasimode (q-TO) which is situated at 410 cm^{-1}. It was decided to compare its intensity with the intensity of the longitudinal part of E1 mode (588 cm^{-1}) and A1(LO) mode - 568 cm^{-1} [40, 41]. The appearance of E1(LO) mode and A1(LO) mode is highly correlated with the angle between the direction of light propagation and the c-axis. The ratio between the q-TO mode and E1(LO) mode shows the area with crystallization in the m-plane. The proportion of the q-TO mode and A1(LO) mode indicates the area with crystallization in the c-plane [33, 40]. The distribution was observed only for the non-annealed sample, where the heat-treated films provided a more homogenous signal.

As can be seen from the cross-section SEM (Fig. 8) pictures of three sol-gel samples, the structure of the annealed film has numerous visible crystallites on their surfaces, which originate from recrystallization. The non-annealed sample is not recrystallized yet - the surface is covered by the fragments of a precursor with the evaporated solvent.

The specific combination of Zn and O into crystallites or the appearance of defects in the structure leads to the creation of additional energetic states. These states can be detected with absorption and photoluminescence measurements. Fig. 9 shows the absorbance spectra of the bulk crystal and thin layers as a function of energy and wavelength. According to the literature [30, 34], the ZnO bulk crystal band-gap value of around 3.4 eV in the room temperature may increase with special doping. As can be seen, the bulk crystal has a shifted absorption edge to significantly lower energies, which is correlated with a considerably higher
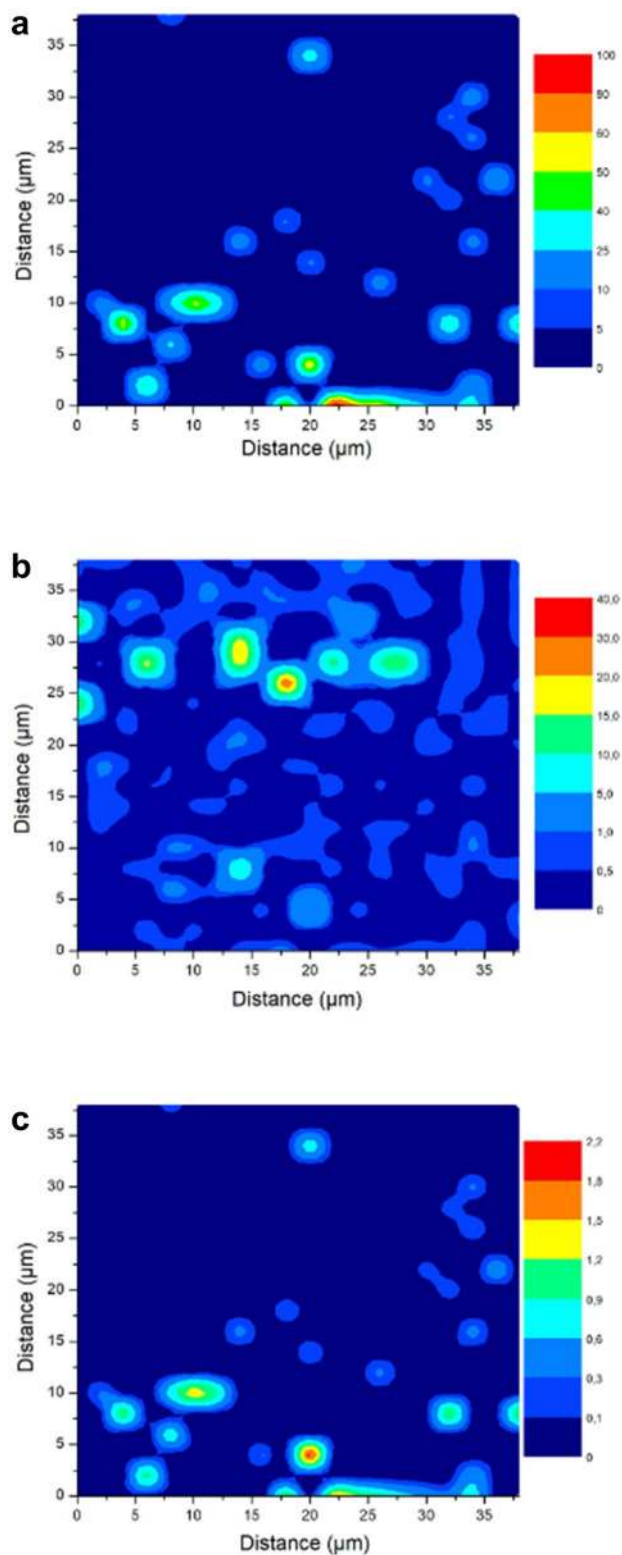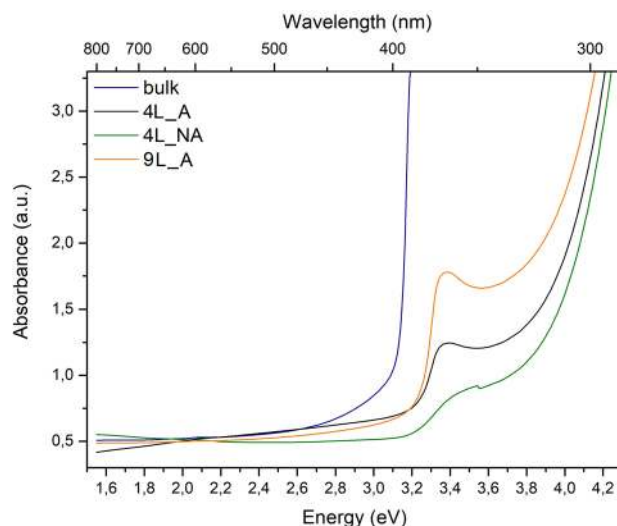
Fig. 7 Raman maps: a, the ratio of the intensity of Raman peaks 410/568 cm^{-1}, b, the ratio of the intensity of peaks 410/588 cm^{-1}, c, the ratio of 2934/1100 cm^{-1}
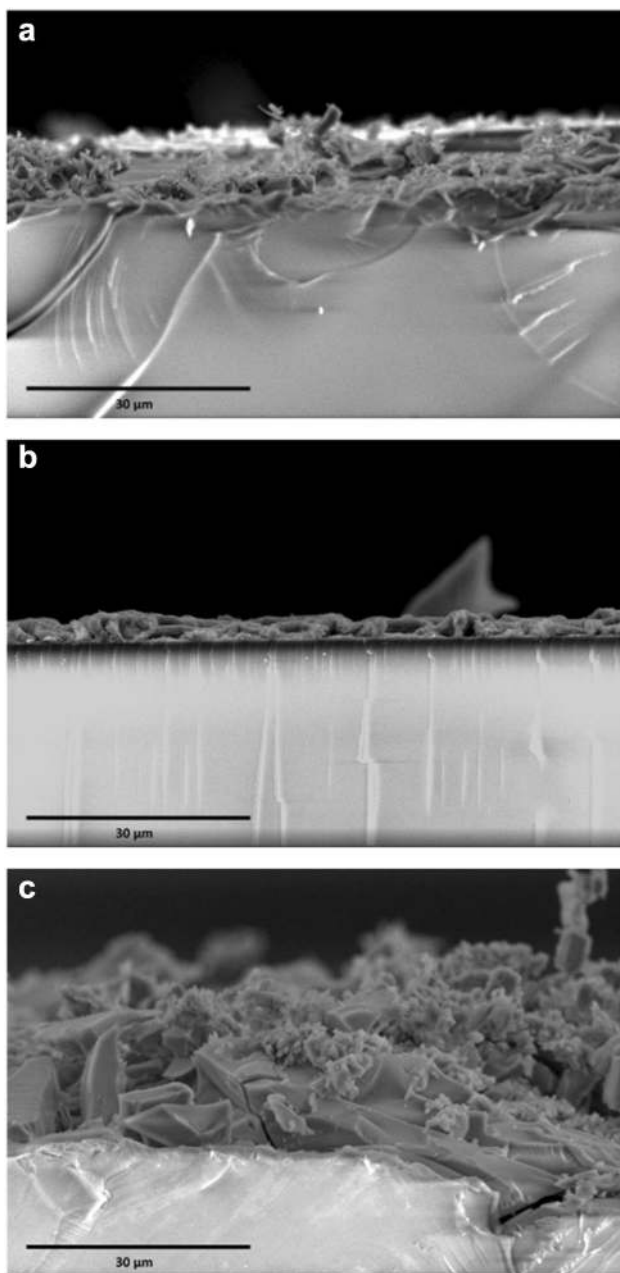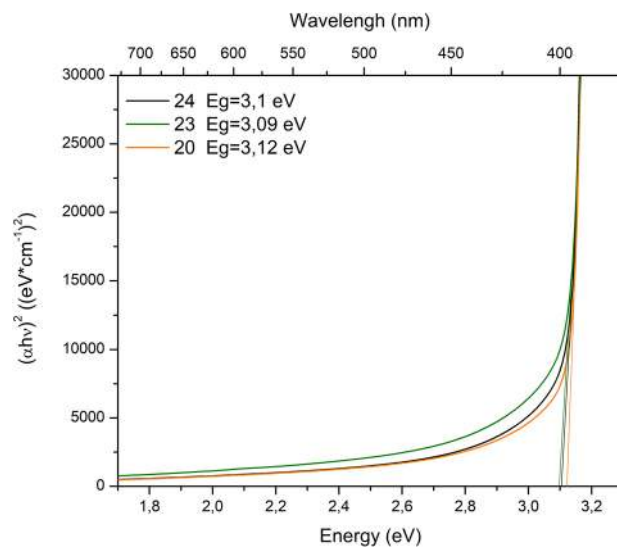
Fig. 8 SEM photos: a, 4L_A sample, b, 4L_NA sample, c, 9L_A sample

Fig. 9 Absorbance registered for all of the analyzed samples

Fig. 10 Tauc plot for three different samples of bulk ZnO

purity of the sample and the atomic rearrangement (the light was perpendicular to c-plane during the measurement). The optical energy band gap, estimated for three different samples with the Tauc Plot (Fig. 10) oscillated between 3.09-3.12 eV. Despite the relatively low-energy bandgap (E_g) value, the obtained result is similar to bandgap calculated for another ZnO crystals grown with the Bridgman method [11, 31, 32]. The absorption edge of the polycrystalline thin films richer in impurities is shifted to notably higher energy, which may indicate the insulating nature of the
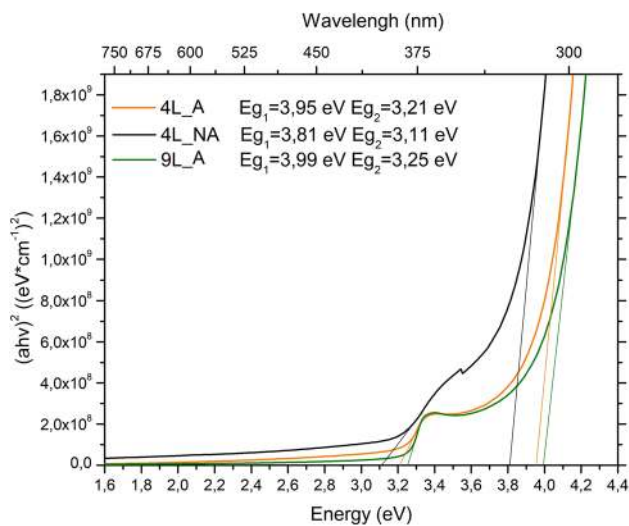
polycrystalline films. The absorption spectra of ZnO layers, despite the absorption edge, exhibit a peak at 3.4 eV. Due to the different orientation of crystallites, the band edge of all thin-film samples divides. This division can be correlated with valence band splitting due to spin-orbit interaction, to band Γ7 and Γ9 [5, 33]. In Fig. 11, Tauc plots for thin films are shown. As may be noticed, the reorientation of crystallites under the annealing caused the decrease of E_g. The Γ7 band also seems to be correlated with the thickness of the samples - a thicker sample exhibits significantly higher energy of electron transition than a thinner sample. Furthermore, the non-annealed sample has a lower forbidden gap than the annealed samples.

Fig. 11 Tauc plot for three different samples of thin films ZnO

Fig. 12 Photoluminescence measurements for thin film samples and bulk crystal

efficiency of photoluminescence of 9 layered films is noticeable higher. Band-to-band recombination peak can be found in both cases in the region of 3.11 - 3.18 eV. The energy of the luminescence of bulk crystal is moderately higher than the energy bandgap calculated with the Tauc plot, which can be explained as a result of an up-conversion mechanism [5, 45]. The peaks in the blue-green region of the luminescence give us valuable information about sample structure. The peaks at 2.87 - 2.82 eV originate from interstitial oxygen, which is a deep acceptor at the octahedral site [46, 47] and the bands at around 2.6 eV could originate from the recombination of electrons and holes on zinc vacancies [46, 47].

The photoluminescence, that arise from excitation with longer wavelengths, may be correlated with the impurities. According to the previous investigation of luminescence resulting from excitement with a wavelength longer than 550 nm [48], red fluorescence may be correlated with carbon doping or organic contamination. The distribution of carbon contamination is shown in the images taken with a confocal microscope in fluorescence mode (Fig. 13), where the brightest regions are the most fluorescent one.
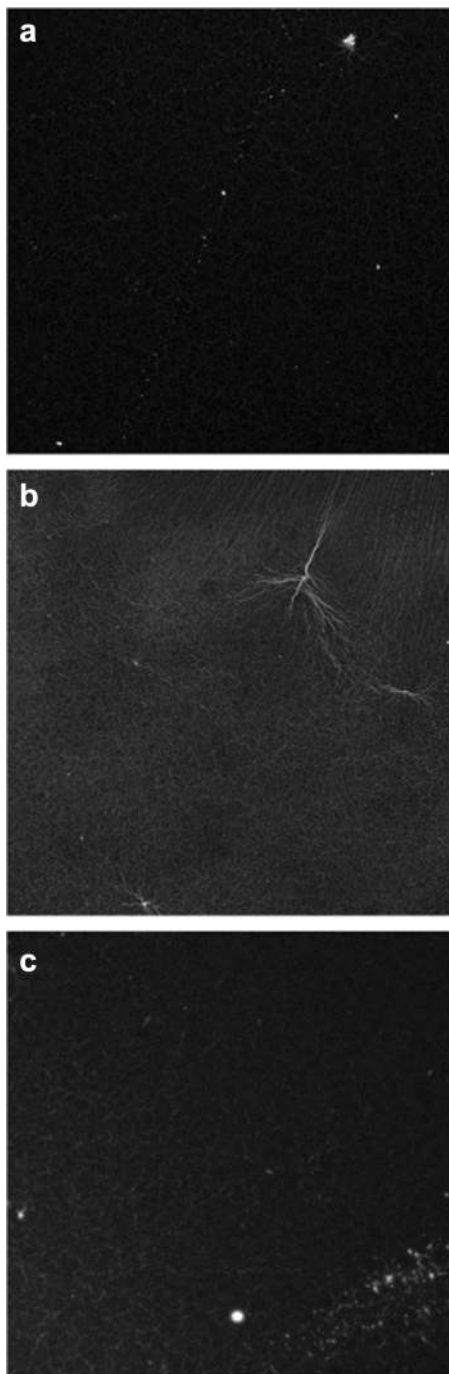
All of the spectrometric measurement results are presented in Table 2.

4 Conclusions

The presented work constitutes the comprehensive analysis of ZnO structures, which may be potentially applied in optoelectronics. The core of the presented research was a comparison of the structural, morphological, and optical properties between self-prepared sol-gel polycrystalline ZnO films and ZnO bulk crystals grown by a Bridgman method.

The morphological and structural properties were investigated using different microscopy techniques, X-ray diffraction, and Raman spectroscopy. The study presented a high influence of annealing on the morphology and crystal structure of thin-film samples. Due to the recrystallization process, the size of crystallites has changed significantly, which had an impact on the physical properties of sol-gel samples, as well as the method of growth, thickness, and size of the samples. In the case of the non-annealed sol-gel layer, the localized reorientation of crystallites was observed with a Raman microscope.

The low-cost sol-gel samples of ZnO showed significantly different properties from bulk crystal. Strongly ordered bulk structure exhibited prominent Raman spectra, relatively low optical energy bandgap, and very low photoluminescence efficiency. Raman, UV-Vis absorption and photoluminescence spectra exhibited by polycrystalline, sol-gel layers were influenced by heterogeneity, different orientation of crystallites, and unintentional doping of the films. These samples have high energy bandgap, which indicates their

It is worth to notice, that a band splitting was also reported in the literature for carbon-doped samples [42, 43], where the downward shift in peak positions was caused by the formation of new Zn-O-C bonds as a result of C_{Zn} defect formation; in this particular case, such feature may originate from organic contamination observed in Raman spectra. The increase of the optical transparency can be attributed to the increase of the porosity and grain size of the ZnO films [44].

In the case of photoluminescence measurements, all samples were excited using 290 nm light and measured in the same ambient conditions. The results are shown in Fig. 12. The intensity of bulk crystals is suppressed, compared to thin films. There are no differences between spectra of 4 layered annealed and non-annealed films although the

Fig. 13 Micrographs made with confocal microscopy in fluorescence mode - for 4L_A (a), 4L_NA (b), 9L_A (c) - made with 20x magnitude objective

Table 2 List of spectroscopic results. Two values of E_g are correlated with the division of a band edge of each thin-film samples (Fig. 11)

Sample	Thickness (μm)	Optical Eg (eV)		Intensity of band-to-band photoluminescence (a.u.)
Bulk crystal	870 ± 1	3.10±0.01		250
4L_A	1.28±0.43	3.95	3.21	1550
4L_NA	1.34±0.41	3.81	3.11	1510
9L_A	1.62±0.53	3.99	3.25	2200

carbon doping or organic residues. Green luminescence was obtained from interstitial oxygen and zinc vacancies.

Compliance with ethical standards

Conflicts of interest We hereby certify that, to the best of our knowledge: 1. No financial support or benefits have been received by us, by any member of our immediate families, or any individual or entity with whom or with which we have a significant relationship from any commercial source which is related directly or indirectly to the scientific work which is reported on in the article except as described below. 2. Moreover, neither we, nor any member of our immediate families, nor any individual or entity with whom or with which we have a significant relationship has a financial interest in the subject matter discussed in the manuscript.

insulating properties. Furthermore, their emission is slightly stronger than the bulk ones.

The study allowed us to estimate the character of defects and contamination in the samples, throughout their spectral properties. Red luminescence, absorption splitting, and organic peaks on Raman spectra pointed an unintentional

References

1. H.E. Ruda, *Widegap II-VI Compounds for Opto-Electronic Applications* (Springer Science, Dordrecht, 1992)
2. J. Millan, P. Godignon, A. Pérez-Tomás, Wide band gap semi-conductor devices for power electronics. Autom. J. Control Meas. Electron. Comput. Commun. **53**, 107–16 (2012)
3. C.F. Klingshirn, ZnO: material, physics and applications. ChemPhysChem **8**, 782 (2007)
4. U. Ozgur, Y.I. Alivov, C. Liu, A. Teke, M.A. Reshchikov, S. Dogan, V. Avrutin, S.J. Cho, H. Morko, A comprehensive review of ZnO materials and devices. J. Appl. Phys. **98**, 1 (2005)
5. C. Klingshirn, J. Fallert, H. Zhou, J. Sartor, C. Thiele, F. Maier-Flaig, D. Schneider, H. Kalt, 65 years of ZnO research - old and very recent results. Phys. Status Solidi **247**, 1424 (2010)
6. O. Schmidt, P. Kiesel, D. Ehrentraut, T. Fukuda, N.M. Johnson, Electrical characterization of ZnO, including analysis of surface conductivity. Appl. Phys. A **88**, 71 (2007)
7. P. Nunes, E. Fortunato, R. Martins, Influence of the post-treatment on the properties of ZnO thin films. Thin Solid Films **383**, 277 (2001)
8. N. Hasuike, T. Harada, T. Kiyohara, K. Nishio, K. Kisoda, H. Harima, Low temperature synthesis of ZnO thin films by spin-coating technique. Phys. Status Solidi C **8**, 506 (2011)
9. V.A. Karpina, V.I. Lazorenko, C.V. Lashkarev, V.D. Dobrowolski, L.I. Kopylova, V.A. Baturin, S.A. Pustovoytov, A.J. Karpenko, S.A. Eremin, P.M. Lytvyn, V.P. Ovsyannikov, E.A. Mazurenko, Zinc oxide:analogue of GaN with new perspective possibilities. Cryst. Res. Technol. **39**, 980 (2004)
10. K. Necib, T. Touam, A. Chelouche, L. Ouarez, D. Djouadi, B. Boudine, Investigation of the effects of thickness on physical properties of AZO sol-gel films for photonic device applications. J. Alloys Compd. **735**, 2236 (2018)
11. D. Schulz, S. Ganschow, D. Klimm, M. Neubert, M. Rossberg, M. Schmidbauer, R. Fornari, Bridgman-grown zinc oxide single crystals. J. Cryst. Growth **296**, 27 (2006)
12. D. Schulz, S. Ganschow, D. Klimm, Melt grown ZnO bulk crystals. Mater. Res. Soc. Symp. Proc. **1201**, 1201 (2010)
13. D. Klimm, S. Ganschow, D. Schulz, R. Fornari, The growth of ZnO crystals from the melt. J. Crystal Growth **310**, 3009 (2008)
14. S. Eisermann, A. Laufer, S. Graubner, M. Pinnisch, J. Stehr, D.M. Hofmann, B.K. Meyer, D. Klimm, D. Schulz, Characterization of ZnO crystals grown by the vertical Bridgman method. Phys. Status Solidi A **208**, 37 (2011)
15. A. Zawadzka, P. Płóciennik, J. Strzelecki, B. Sahraoui, Transparent amorphous zinc oxide thin films for NLO applications. Opt. Mater. **37**, 327 (2014)
16. S. Kim, H. Yoon, D.Y. Kim, S.O. Kim, J.Y. Leem, Optical properties and electrical resistivity of boron-doped ZnO thin films grown by sol-gel dip-coating method. Opt. Mater. **35**, 2418 (2013)
17. W. Bala, Y. Zorenko, V. Savchyn, T. Voznyak, K. Paprocki, P. Popielarski, M. Szybowicz, Optical and electrical properties of ZnO thin films grown by Sol-Gel method. Solid State Phenom. **200**, 14 (2013)
18. R. Mahendran, M. Kashif, M. Saroja, M. Venkatachalam, C. Sanjeeviraja, U. Hashim, Structural and optical characterization of ZnO thin films annealed at different temperatures. J. Appl. Sci. Res. **9**, 5460–7 (2013)
19. L. Znaidi, T. Touam, D. Vrel, N. Soudeda, S. Ben Yahiaa, O. Brinzaa, A. Fischerb, A. Boudrioua, ZnO thin films synthesized by sol-gel process for photonic applications. Acta Phys. Pol. A **121**, 165 (2012)
20. L. Znaidi, Sol-gel-deposited ZnO thin films: a review. Mater. Sci. Eng. B **174**, 18 (2010)
21. M. Sahal, B. Hartiti, A. Ridah, M. Mollar, B. Marí, Structural, electrical and optical properties of ZnO thin films deposited by sol-gel method. Microelectron. J. **39**, 1425 (2008)
22. R. Ghosh, B. Mallik, S. Fujihara, D. Basak, Photoluminescence and photoconductance in annealed ZnO thin films. Chem. Phys. Lett. **403**, 415 (2005)
23. K. Ravichandran, M. Vasanthi, K. Thirumurugan, B. Sakthivel, K. Karthika, Annealing induced reorientation of crystallites in Sn doped ZnO films. Opt. Mater. **37**, 59 (2014)
24. A. Purohit, S. Chander, A. Sharma, S.P. Nehra, M.S. Dhaka, Impact of low temperature annealing on structural, optical, electrical and morphological properties of ZnO thin films grown by RF sputtering for photovoltaic applications. Opt. Mater. **49**, 51 (2015)
25. S.A. Kamaruddin, K.Y. Chan, H.K. Yow, M.Z. Sahdan, H. Saim, D. Knipp, Zinc oxide films prepared by sol-gel spin coating technique. Appl. Phys. A **104**, 263 (2011)
26. J. Humphreys, G.S. Rohrer, *Recrystallization and Related Annealing Phenomena* (Elsevier, Amsterda, 2017)
27. D.K. Pandey, K. Ghosh, S. Mishra, J.P. Bange, P.K. Bajpai, Effect of film thickness on structural and optical properties of sol-gel spin coated aluminum doped zinc oxide (Al:ZnO) thin films. Mater. Res. Express (2018). https://doi.org/10.1088/2053-1591/aad3a8
28. H. Moroc, U. Ozgur, *General Properties of ZnO, Zinc Oxide: Fundamentals, Materials and Device Technology* (WILEY- VCH Verlag GmbH and Co. KGaA, Weinheim, 2009)
29. B. Ghosh, S.C. Ray, M. Pontsho, S. Sarma, D.K. Mishra, Y.F. Wang, W.F. Pong, A.M. Strydom, Defect induced room temperature ferromagnetism in single crystal, poly-crystal, and nanorod ZnO: a comparative study. J. Appl. Phys. **123**, 161507 (2018)
30. L. Bergman, X.B. Chen, J. Huso, J.L. Morrison, H. Hoeck, Raman scattering of polar modes of ZnO crystallites. J. Appl. Phys. **98**, 093507 (2005)
31. K. Gas, Właściwości Strukturalne, optyczne i dynamiczne sieci monokryształów ZnO i nanodrutów typu rdzeń-powłoka na bazie ZnTe, Instytut Fizyki Polskiej Akademii Nauk, Warszawa [PhD Thesis - Structural, optical and dynamic properties of ZnO single crystal and core-shell nanowires based on ZnTe, Institute of Physics of the Polish Academy of Sciences, Warsaw] (2013)
32. T.C. Damen, S.P.S. Porto, B. Tell, Raman effect in zinc oxide. J. Phys. Chem. Solids Mitra **142**, 1085 (1966)
33. R. Loudon, The Raman effect in crystals. Adv. Phys. **13**, 423 (1964)
34. C. Klingshirn, ZnO: from basics towards applications. Phys. Status Solidi B **244**, 3027 (2007)
35. S. Jabri, H. Souissi, A. Souissi, A. Meftah, V. Sallet, A. Lusson, P. Galtier, M. Oueslati, Investigation of the vibrational modes of ZnO grown by MOCVD on different orientation planes. J. Raman Spectrosc. **46**, 251 (2015)
36. S.A. Studenikin, N. Golego, M. Cocivera, Fabrication of green and orange photoluminescent, undoped ZnO films using spray pyrolysis. J. Appl. Phys. **84**, 2287 (1998)
37. P.A. Rodnyi, I.V. Khodyuk, Optical and luminescence properties of zinc oxide. Opt. Spectrosc. **111**, 776 (2011)
38. J.H. Cai, G. Ni, G. He, Z.Y. Wu, Red luminescence in ZnO films prepared by a glycol-based Pechini method. Phys. Lett. A **372**(22), 4104–4108 (2008)
39. S.T. Tan, X.W. Sun, Z.G. Yu, P. Wu, G.Q. Lo, D.L. Kwong, p-type conduction in unintentional carbon-doped ZnO thin films. Appl. Phys. Lett. **91**, 91 (2007)
40. N. Ashkenov, B.N. Mbenkum, C. Bundesmann, V. Riede, M. Lorenz, D. Spemann, E.M. Kaidashev, A. Kasic, M. Schubert, M. Grundmann, G. Wagner, H. Neumann, V. Darakchieva, H. Arwin, B. Monemar, Infrared dielectric functions and phonon modes of high-quality ZnO films. J. Appl. Phys. **93**, 126 (2003)

41. A. Zaoui, W. Sekkal, Pressure-induced softening of shear modes in wurtzite ZnO: a theoretical study. Phys. Rev. B **66**, 1 (2002)

42. M. Samadi, M. Zirak, A. Naseri, E. Khorashadizade, A.Z. Moshfegh, Recent progress on doped ZnO nanostructures for visible-light photocatalysis. Thin Solid Films **605**, 2 (2016)

43. R. Mohammadigharehbagh, S. Pat, S. Özen, H.H. Yudar, Ş. Korkmaz, Investigation of the optical properties of the indium-doped ZnO thin films deposited by a thermionic vacuum arc. Optik **157**, 667 (2018)

44. L. Ouarez, A. Chelouche, T. Touam, R. Mahiou, D. Djouadi, A. Potdevin, Au-doped ZnO sol-gel thin films: an experimental investigation on physical and photoluminescence properties. J. Lumin. **203**, 222 (2018)

45. K.N. Shinde, S.J. Dhoble, H.C. Swart, K. Park, *Basic Mechanisms of Photoluminescence (Phosphate Phosphors for Solid-State Lighting)* (Springer, Berlin, 2012)

46. A. Janotti, C.G. Van De Walle, New insights into the role of native point defects in ZnO. J. Crystal Growth **287**, 58 (2006)

47. A. Janotti, C.G. Van De Walle, Fundamentals of zinc oxide as a semiconductor. Rep. Progress Phys. **72**, 1 (2009)

48. L. Ke, S.C. Lai, J.D. Ye, V.L. Kaixin, S.J. Chua, Point defects analysis of zinc oxide thin films annealed at different temperatures with photoluminescence. Hall mobility, and low frequency noise. J. Appl. Phys. **108**, 1 (2010)